Experimental Modal Analysis of Rectangular and Circular Beams

B. H. Emory and W. D. Zhu

University of Maryland, Baltimore County

1. INTRODUCTION

The main focus of this work is to develop two test stands and accompanying activity to teach undergraduate and graduate students about vibrations and experimental modal analysis. Currently our department does not have an instructional module that can be used to educate students on how to perform modal testing and use modern vibrations and modal testing equipment and software. Within modal testing there are many mistakes that can be made, which are not noticed when doing computer simulation using finite element software. A few simple mistakes include choice of the wrong accelerometer location, improper accelerometer mounting, choice of the wrong exciter tip, impacting the structure with too much force that would overload the instruments, double impacts, and improper setup of the data collection equipment and software. Laboratory-based engineering education is important because "engineering students see themselves as essentially practical" [1]. Laboratory experience is critical to a student's development because unlike computer simulation, laboratory work teaches students that attention to detail is paramount. It is also important to remember that engineers will always be responsible for their actions and that an education, which separates them in any way from reality, introduces danger [2].

The test stand developed for a rectangular beam provides different sets of boundary conditions. It can be used for undergraduate and graduate education as well as other experiments in the laboratory. For example, it can be used to validate a robust, iterative algorithm for structural damage detection [3] and the optimal damper location that can dissipate the largest number of modes of a beam [4]. The test stand could also be used to complement computational simulations like the one presented by Pota and Alberts [5]. The boundary conditions are studied by comparing the natural frequencies and mode shapes from experimental measurements with those predicted using the Euler-Bernoulli beam theory. In many vibrating beam or plate experiments there is no discussion of validity of boundary conditions [6-9]. The effect of the sensor location is demonstrated along with that of the torque in the bolts used to secure the rectangular beam at the clamped and pinned boundaries. In many cases there is no discussion of accounting for mass loading by the sensor and determining its placement before testing [6-8]. Proper selection of the exciter tip is also addressed by examining the measured frequency response function (FRF) and coherence.

Knowledge of material properties, such as the elastic modulus, shear modulus, and Poisson's ratio, are important in mechanical design and research. Determination of the material properties of a specimen is important since they vary from one to another. Vibration testing is preferred over destructive testing because the specimen can be used in further experimentation. Vibration testing is also advantageous for material property testing because it is less costly than using a tensile or torsion test. A circular beam test stand is presented for material property testing because the torsional equation of motion is exact for the circular beam. A new apparatus is used for measuring the torsional vibration of the circular beam with an accelerometer [10]. Free-free boundary conditions are used because they are more easily verifiable than other boundary conditions. The linear curve-fit method [11] is used to determine the material properties. The Timoshenko and Euler-Bernoulli beam theories for the bending modes are compared to determine which theory gives more accurate results. Students can gain a wide range of experience in modal testing by performing similar experiments with the test stands.

2. EXPERIMENTAL SETUP

To perform modal testing a personal computer is used to control and collect data from a dynamic signal analyzer (Siglab Model 20-42). Inputs from the accelerometer (PCB U352C66) and impact hammer (PCB Model 086C01) are conditioned using a signal conditioner (PCB Model 482A17). In order

Abstract

Analytical and experimental methods are used to determine the natural frequencies and mode shapes of Aluminum 6061-T651 beams with rectangular and circular cross-sections. A unique test stand is developed to provide the rectangular beam with different boundary conditions including clamped-free, clamped-clamped, clamped-pinned, and pinned-pinned. The first 10 bending natural frequencies and mode shapes for each set of boundary conditions are measured. The effect of the bolt torque on the measured natural frequencies is examined. A new technique is used to mount an accelerometer on the circular beam to measure its torsional modes; its first 20 natural frequencies and first 10 mode shapes are measured. The measured natural frequencies and mode shapes of both beams are compared with their theoretical predictions. The Timoshenko beam theory is shown to provide better predictions of the higher bending natural frequencies of the circular beam than the Bernoulli-Euler beam theory. The material properties of the circular beam, including the elastic modulus, shear modulus, and Poisson's ratio, are determined accurately. The use of the rectangular and circular beam test stands as a teaching tool for undergraduate and graduate students is discussed. The laboratory demonstration using the test stands was well received by students in the undergraduate vibrations class.

KEYWORDS: modal testing, Timoshenko beam theory, material property measurement, educational laboratories

to measure all the frequencies in a given bandwidth, the sampling frequency ω_s needs to be at least twice the maximum frequency to be measured. Otherwise aliasing will occur. In Siglab the sampling frequency is 2.56 times the bandwidth. In all experiments in this work the bandwidth starts at the zero frequency and aliasing will not occur. To obtain the desired frequency resolution *dF*, the record length *RL* in the time domain is chosen to be $RL = \frac{\omega_s}{dF}$. The bandwidth is adjusted to give the desired accuracy.

Care should be taken in selecting the record length. When the record length is too short, the vibration of the structure does not dissipate fully, which causes leakage. Applying a windowing function to the response signal helps to force the signal to zero near the end of the measurement, which reduces leakage. Another advantage of this windowing function is that it places more weight on the initial part of the signal than the latter. While the use of the exponential window in Siglab can affect the measurement of damping ratios of the structure, it does not affect the measurement of its natural frequencies and mode shapes. A boxcar window is used for the input.

While testing over different frequency ranges the hammer tip is changed accordingly. At low frequencies an extender is used for the hammer. For all experiments, only one accelerometer with 2 gram mass is used to keep mass loading to a minimum. For every impact test three impacts are averaged to ensure repeatable results and to obtain a coherence measurement. The accelerometer is affixed to the specimen using Petro wax.

3. RECTANGULAR BEAM

The rectangular beam has a cross-section of .0761 m by .0065 m and a total length of .916 m. Its mass density is 2715 kg/m^3. The boundary conditions are composed of steel clamps with an aluminum base and can be configured to impose clamped (Fig. 1) or pinned (Fig. 2) conditions. The beam has a length of .861 m, .812 m, 860 m, and .912 m when subjected to the clamped-free, clamped-clamped, clamped-pinned, and pinned-pinned boundary conditions, respectively. There are five main parts to each boundary, including the aluminum base plate (Fig. 3), steel-threaded base (Fig. 4), steel pin base (Fig. 5), 95.25 mm bolts, and 190.5 mm bolts. The aluminum base plate allows for the steel-threaded base to be mounted to it in a variety of positions. The base is made to accommodate various fixtures, some of which are not utilized in this work. The steel-threaded base has two sets of threads to receive the 190.5 mm bolts. Steel is used because torque is applied to the bolts; boundary conditions made of aluminum can be ruined after torquing a few times. The clamped or pinned boundaries are secured with two 190.5 mm bolts, the steel-threaded base is fastened to the aluminum base with 95.25 mm bolts, and the aluminum base is secured to an optical table using five 95.25 mm bolts. Once the boundary condition type is chosen, a torque wrench is used to ensure that both bolts have nearly the same torque and that the boundary does not impose a moment on the beam; a level can also be used on top of the boundary for this purpose. A level is important when setting up a pinned boundary as very little torque is needed.

The first experiment conducted on the beam is to determine the amount of torque at which the first natural frequency of the clamped-free rectangular beam becomes constant. The impact and accelerometer locations remain fixed in this experiment, and the extender is used for the hammer as the bandwidth is from 0 to 10 Hz. For the first test the nuts are only screwed down so that the bottom of the nut touches the top steel bar (hand-tight). The torque is increased in increments of 6.8 Nm and an impact test is performed accordingly.

When using a clamped boundary condition, the bolts are torqued to 40.7 Nm. For a pinned boundary condition the bolts are only hand-tightened so that the top bar does not rotate but the beam can still rotate. Tightening the bolts more than hand-tight can make the pin cut into the beam and change the boundary from pinned to clamped. The pinned boundary condition is also modeled physically by allowing as little of the beam as possible to extend past the pinned end because the weight of the extended portion of the beam creates a moment at the pinned end.

The next experiment is to locate the accelerometer so that it has a minimal effect on the first natural frequency while achieving the desired coherence for the clamped-free beam. The extender is used as the bandwidth is from 0 to 10 Hz. The optimum location of the accelerometer is found by impacting the beam in the same location while moving the accelerometer from the free end to the clamped end of the beam. Once a range is found in which the accelerometer has little effect on the first natural frequency, the coherence can be improved by moving the hammer closer

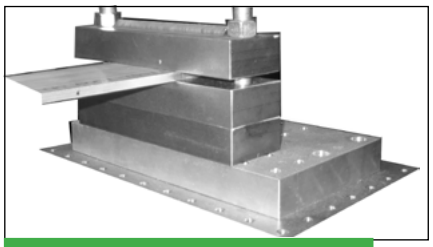

Fig. 1 Clamped boundary condition

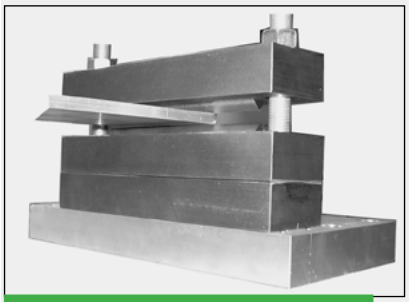

Fig. 2 Pinned boundary condition

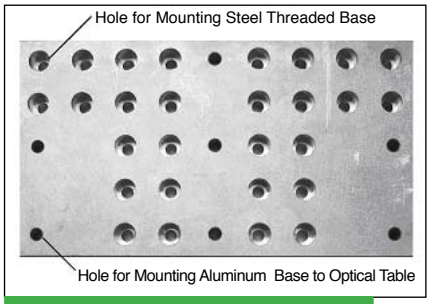

Fig. 3 Bottom view of the aluminum base

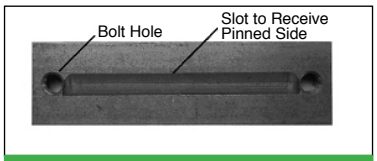

Fig. 4 Top view of the threaded steel base

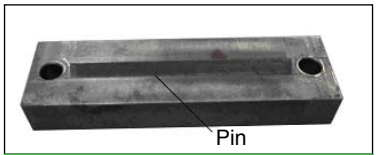

Fig. 5 Overview of the pinned base

or farther away from the accelerometer. The location of the impact is important as exciting the beam close to the boundary will excite the high modes while exciting the beam near the free end will excite the low modes. The amplitude of the response is also important in determining the best placement of the accelerometer as increasing the amount of output due to the input reduces the effect that noise has on the measurement. For all tests coherence over .98 at resonance is considered to be necessary for accurate measurements since the structure being tested is very simple. Coherence is also taken into account when determining the optimal sensor placement because coherence decreases as the accelerometer is moved closer to the boundary. This occurs because the amplitude of vibration decreases and noise contributes to more of the signal.

A set of experiments is also conducted to determine which hammer tip is the best for the frequency range tested. For the same impact and accelerometer locations a variety of hammer tips are tested. The tip selection is important. If the tip is too hard it will excite higher modes than desired. Since not all of the energy input into the system is used in exciting the modes to be measured, the coherence will be low for lower modes. The opposite is true for a soft tip not exciting higher modes.

The bending natural frequencies of the beam are measured by placing the accelerometer at the middle of the beam widthwise to eliminate any torsional modes from the FRF. Each impact test is conducted at the middle of the beam widthwise to ensure that no torsional modes are excited as well. Care is taken to avoid nodal points while testing to keep the amplitude of the response measured much greater than the noise level. To obtain a mode shape of the beam, a roving hammer test is conducted at equally spaced positions along the length of the beam, keeping the same sensor location for each test. For each beam more impact locations than the highest desired mode number are used to ensure that the full shape can be captured. ME'Scope VES is then used to do curve fitting on the FRFs to generate the complex mode shape vector for each experimental mode. The mode shape vector is complex due to the existence of light natural damping.

To determine the correlation of the experimental and theoretical (see Appendix A) mode shapes, the modal assurance criterion (MAC) is used to determine the deviation between them, which is defined as [11]

$$MAC = \frac{\left|\sum_{j=1}^{m}(\psi_E)_j(\psi_T)_j^*\right|^2}{\left(\sum_{j=1}^{m}(\psi_E)_j(\psi_E)_j^*\right)\left(\sum_{j=1}^{m}(\psi_T)_j(\psi_T)_j^*\right)} \quad (1)$$

where $(\psi_E)_j$ and $(\psi_T)_j$ are the j-th component of the experimental and theoretical mode shape vectors, respectively, of dimension m, and the superscript * denotes complex conjugation. Note that the undamped, theoretical natural frequencies and mode shapes are compared with the damped, experimental natural frequencies and mode shapes, respectively. Note also that the MAC numbers given in Tables 3 through 6 and in Table 8 have been multiplied by 100.

To determine the elastic modulus, the theoretical natural frequencies of the bending modes from the Euler-Bernoulli beam theory (Appendix A) are plotted against the corresponding experimental ones. The resulting line from a linear curve fit should have a slope of one [11]. If the line has a slope greater than one, the assumed elastic modulus in obtaining the theoretical results is too large and needs to be lowered until the theoretical verse experimental line has a slope of one, and vice versa.

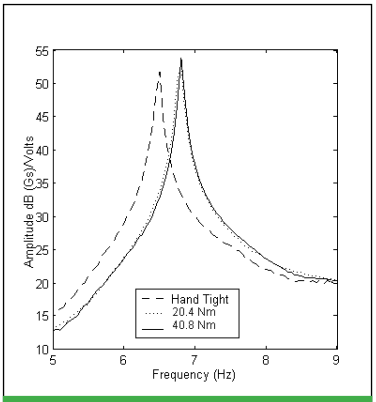

Fig. 6 FRF of the clamp-free beam with different bolt torques

4. RESULTS AND DISCUSSION FOR THE RECTANGULAR BEAM

The effect of the sensor location on the first natural frequency of the clamped-free beam is shown in Table 1, where the boundary at x=0 is clamped. It is seen that the natural frequency increases as the accelerometer is moved closer to the clamped boundary, which shows that the effect of mass loading from the accelerometer decreases. The FRF in the neighborhood of the first natural frequency of the clamped-free beam at various torque levels is shown in Figure 6. When the torque applied to the bolts is increased, the natural frequency increases until the torque reaches 27 Nm. Ensuring the bolt

Position (m)	Frequency (Hz)
0.085	6.81
0.255	6.81
0.510	6.81
0.595	6.80
0.681	6.79
0.776	6.79
0.861	6.78

Table 1 First natural frequency of the clamped-free beam for various sensor positions

C-F Exp. (Hz)	C–F Theo. (Hz)	Error %	C-C Exp. (Hz)	C-C Theo. (Hz)	Error %
6.8	7	-2.9	47.8	50.1	-4.8
42.8	43.9	-2.6	130.3	138.1	-6
120	122.9	-2.4	257.8	270.8	-5
232.2	240.8	-3.7	437.5	447.6	-2.3
397.8	398.1	-0.1	666.6	668.6	-0.3
588.1	594.7	-1.1	899	933.9	-3.9
818.4	830.6	-1.5	1207	1243	-3
1092	1106	-1.3	1541	1597	-3.6
1402	1420	-1.3	1925	1995	-3.6
1757	1774	-1	2356	2437	-3.4

P-C Exp. (Hz)	P-C Theo. (Hz)	Error %	P-P Exp. (Hz)	P-P Theo. (Hz)	Error %
29.7	30.8	-3.7	18.1	17.5	3.3
96.9	99.8	-3	70.6	70.1	0.7
203.1	208.1	-2.5	160	157.7	1.4
362.5	355.9	1.8	276.9	280.4	-1.3
531.3	543.1	-2.2	440	438.1	0.4
754.7	769.7	-2	630.6	630.8	0
1008	1036	-2.8	856.3	858.6	-0.3
1303	1341	-2.9	1083	1121	-3.5
1740	1686	3.1	1408	1419	-0.8
2082	2070	0.6	1756	1752	0.2

Table 2 Theoretical and experimetal natural frequencies of the first 10 bending modes of the rectangular beam (C=Clamped, F=Free, and P=Pinned)

torque above this threshold value is important in approximating a clamped boundary. Note that the peak amplitude in Figure 6 also increases slightly with the bolt torque due to reduced damping.

The measured bending natural frequencies of the rectangular beam subjected to each set of boundary conditions are given in Table 2 along with the natural frequencies computed using the Euler-Bernoulli beam theory. The boundary conditions are considered to be good approximations of their theoretical models since all theoretical versus experimental natural frequency plots yield an elastic modulus near 67 GPa; the slopes of the resulting lines in Fig. 7 from the linear curve-fit are all nearly one.

The MAC matrix for each set of boundary conditions is given in Tables 3 through 6. Each column of the MAC matrix represents one experimental mode compared with all theoretical modes and each row represents the opposite. From the MAC matrices it is seen that there is good correlation between the theoretical and experimental results since all MAC numbers are above 90% for the same theoretical and experimental modes and less than 10% for different ones. The normalized experimental mode shapes from ME'Scope VES for the first ten bending modes of the clamped-free beam are plotted with the corresponding theoretical mode shapes in Figure 8.

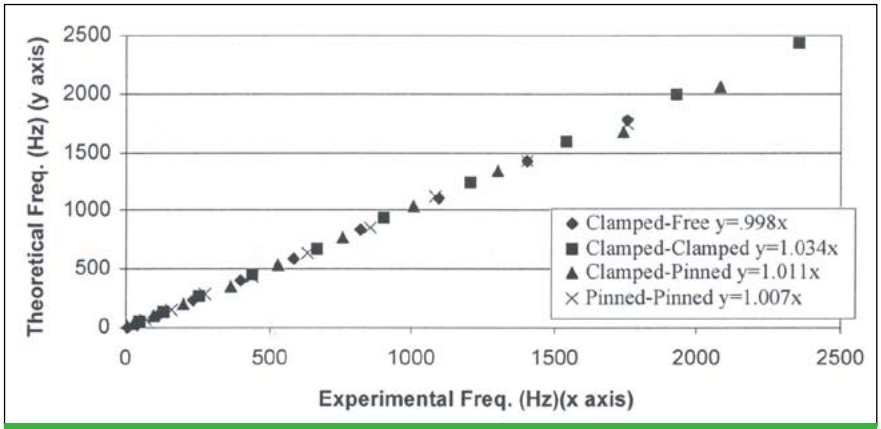

Fig. 7 Theoretical versus experimental natural frequencies of the rectangular beam

Plots of the FRF and coherence associated with a soft, medium, and hard tip used to excite the clamped-free beam are shown in Fig. 9. In Fig. 9a the tip used is too soft, the higher modes are not fully excited, and the FRF is very jagged. The coherence for the higher modes in Fig. 9b is less than .98 and jagged due to poor excitation of the higher modes. The FRF from the correct exciter tip is smooth throughout the measurement bandwidth, and the coherence drops below .98 only when there is an anti-resonance. Figure 9c is the result of using an exciter tip that is too hard, because the coherence near each of the first four natural frequencies is less than .98.

5. CIRCULAR BEAM

The circular beam has a diameter of .0191 m, a length of 0.796 m, and the same mass density as that of the rectangular beam. Free-free boundary conditions are approximated using thin threads (Fig. 10). To validate the free-free boundary conditions, the natural frequencies corresponding to the rigid-body modes are ensured to be within 10% of the first bending mode. The threads are attached to the ends of the beam as shown in Fig. 10. The locations of the threads are chosen for convenience here since the best locations for the threads would be at the nodal points. The bending vibration of the circular beam is measured by affixing the accelerometer to the circumference of the beam. The accelerometer is placed near but not at the center of the beam to avoid a nodal point of the even modes. To measure the longitudinal vibration, the accelerometer is affixed to an end of the beam perpendicular to the face. Measurement of the torsional vibration presents a challenge as the accelerometer

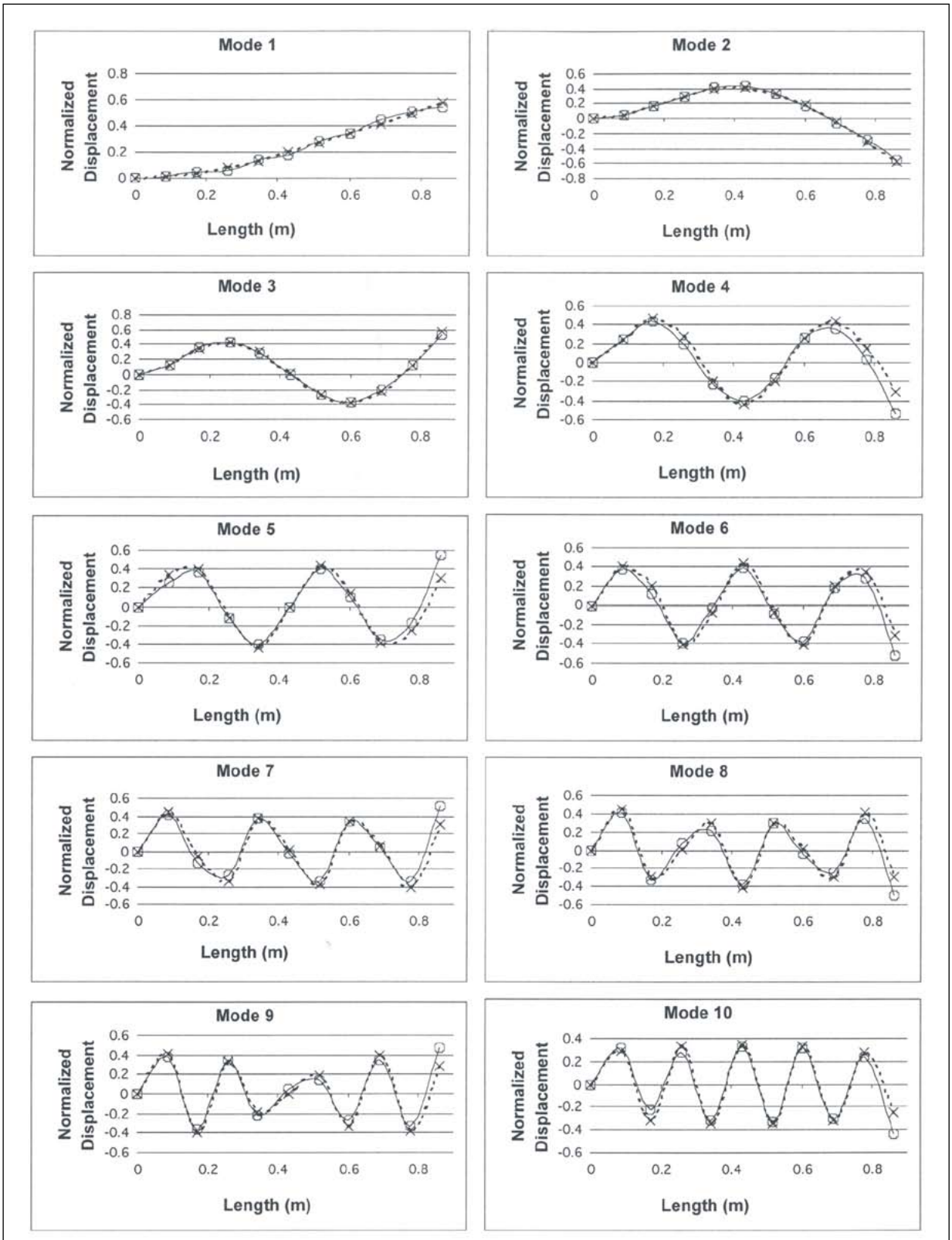

Fig. 8 The first ten theoretical (dashed line, -x-) and experimental (solid line, -o-) bending mode shapes of the clamped-free rectangular beam

Exp. Mode	Theoretical Mode Number 1	2	3	4	5	6	7	8	9	10
1	99.5	3.1	2.8	2.9	3.2	3.4	3.5	4.2	4.1	3.7
2	2.8	99.4	3.5	2.8	4.4	3.5	3.7	3.9	3.9	4.2
3	2.8	3.0	99.7	5.7	4.3	5.1	4.1	4.3	4.6	3.4
4	0.5	0.1	0.0	92.4	1.5	0.5	1.7	1.4	1.0	2.0
5	0.0	0.2	0.4	0.0	92.2	2.5	0.7	1.5	2.2	0.4
6	0.0	0.5	0.3	1.0	1.3	93.5	3.1	1.1	1.3	3.3
7	0.1	0.3	0.5	0.5	0.7	0.5	93.6	2.9	2.2	0.5
8	0.2	0.6	0.9	1.1	1.6	2.1	0.3	93.5	2.3	3.7
9	0.4	1.0	0.7	1.0	1.3	1.1	3.6	0.0	94.7	2.0
10	0.9	0.6	0.9	1.1	1.6	2.0	0.6	5.2	0.0	95.3

Table 3 Clamped-free beam MAC matrix

Exp. Mode	Theoretical Mode Number 1	2	3	4	5	6	7	8	9	10
1	99.3	0.0	0.1	0.7	0.0	0.0	0.0	0.0	0.2	0.0
2	0.2	99.7	0.0	0.1	0.2	0.1	0.0	0.4	0.0	0.0
3	0.3	0.5	97.1	1.8	0.6	1.1	0.9	0.3	0.4	0.0
4	0.1	0.0	0.1	97.2	0.1	1.1	0.0	0.3	0.5	0.3
5	0.2	0.0	0.0	0.0	98.2	0.1	0.7	0.0	0.0	0.6
6	0.1	0.0	0.0	0.0	0.1	97.9	0.7	0.4	0.1	0.6
7	0.0	0.0	0.0	0.1	0.2	0.0	97.0	0.1	0.0	0.7
8	0.1	0.0	0.1	0.1	0.0	0.7	0.7	97.7	0.1	0.4
9	0.0	0.0	0.0	0.2	0.2	0.0	1.4	0.5	99.3	0.1
10	0.1	0.0	0.1	0.0	0.2	0.5	0.2	3.2	0.1	98.5

Table 4 Clamped-clamped beam MAC matrix

Exp. Mode	Theoretical Mode Number 1	2	3	4	5	6	7	8	9	10
1	97.5	0.0	0.0	0.0	0.1	0.0	0.1	0.1	0.0	0.0
2	0.2	99.0	0.3	0.3	1.0	0.0	0.3	0.0	0.3	0.2
3	0.2	0.3	98.2	0.4	0.5	0.3	0.1	0.1	0.0	0.1
4	0.2	0.4	0.6	95.7	1.0	0.1	0.2	0.5	0.1	0.0
5	0.2	0.2	0.4	1.2	93.8	0.5	1.5	0.4	0.0	0.3
6	0.0	0.0	0.1	1.3	2.0	97.1	2.1	3.1	0.0	0.6
7	1.1	0.0	0.1	0.5	1.2	1.0	90.7	1.1	0.0	0.1
8	0.0	0.1	0.1	0.5	0.3	0.4	3.0	93.6	1.1	0.0
9	0.4	0.0	0.0	0.4	0.2	0.8	1.7	0.3	95.4	1.1
10	0.1	0.1	0.0	0.2	0.3	0.7	1.5	0.8	4.8	95.6

Table 5 Clamped-pinned beam MAC matrix

Exp. Mode	Theoretical Mode Number 1	2	3	4	5	6	7	8	9	10
1	99.8	0.0	0.0	0.1	0.0	0.0	0.3	0.0	1.1	0.1
2	0.0	99.9	0.0	0.1	0.1	0.0	0.2	0.3	0.0	1.4
3	0.1	0.0	99.2	0.4	0.0	0.2	0.1	0.2	0.1	0.2
4	0.0	0.0	0.1	98.3	0.6	0.1	0.3	0.0	0.1	0.2
5	0.0	0.0	0.2	1.0	98.6	0.5	0.5	0.5	0.0	0.9
6	0.0	0.0	0.1	0.2	0.5	98.5	1.2	0.0	0.5	1.3
7	0.0	0.0	0.0	0.0	0.1	0.7	94.9	2.9	3.6	1.4
8	0.0	0.0	0.0	0.0	0.1	0.0	1.8	93.7	2.1	2.2
9	0.0	0.0	0.4	0.0	0.0	0.0	0.4	2.0	91.1	3.5
10	0.0	0.0	0.0	0.0	0.0	0.0	0.1	1.0	1.6	90.7

Table 6 Pinned-pinned beam MAC matrix

needs to be affixed tangentially to the beam. To this end, a bracket is made by bending a thin steel band around the beam, leaving a tab for the accelerometer (Fig. 11) [10]. The bracket is attached to the beam using Petro wax. This system works because the natural frequencies of the bracket are much higher than those of the beam. A roving hammer test is used to measure the mode shapes.

To determine the elastic modulus, the theoretical bending natural frequencies from the Timoshenko beam theory (see Appendix B) are plotted against their measured ones. The elastic modulus can also be determined by comparing experimental and theoretical (see Appendix C) longitudinal natural frequencies [10], which is an easier method. The same approach is used for the experimental and theoretical (see Appendix C) torsional natural frequencies to determine the shear modulus. The Poisson's Ratio, ν, is then determined from

$$\nu = \frac{E}{2G} - 1 \qquad (2)$$

where E is the elastic modulus and G is the shear modulus.

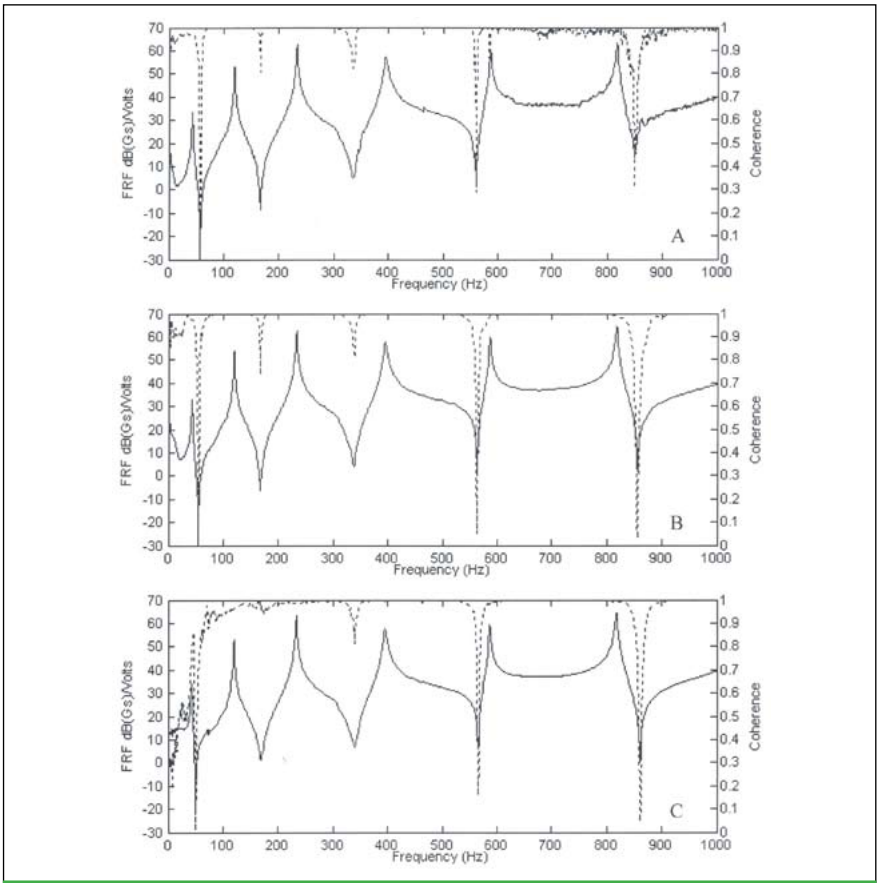

Fig. 9 FRF (solid line, ——) and coherence (dashed line, ---) using (A) the soft tip, (B) the correct tip, and (C) the hard tip.

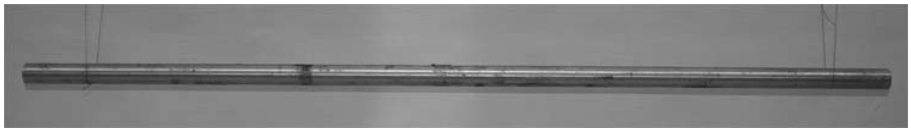

Fig. 10 Free boundary conditions of the circular beam

Fig. 11 Accelerometer bracket used for torsional vibration measurement

6. RESULTS AND DISCUSSION FOR THE CIRCULAR BEAM

The natural frequencies corresponding to the rigid-body modes are measured to be 6.25 Hz and 12.5 Hz, respectively. The boundary conditions are considered to be a valid approximation of their theoretical model because the highest rigid-body mode frequency is 9% of the first bending mode, which is smaller than 10-20% limit defined in [11]. Figure 12 compares the experimental natural frequencies with the theoretical ones. The elastic and shear moduli of the beam are determined to be 70.5 GPa and 26.45 GPa, respectively, with a Poisson's ratio of .333. The measured Poisson's ratio for Aluminum 6061-T651 is in excellent agreement with its published value of 0.33 [12]. Using the ASTM testing procedure [13] in a previous study [14] yields relatively large measurement errors for the Poisson's ratio. The resulting line from the linear curve fit of the theoretical and experimental bending natural frequencies has a slope of .995 and that from the linear curve fit of the theoretical and experimental torsional natural frequencies has a slope of .998 (Fig 12).

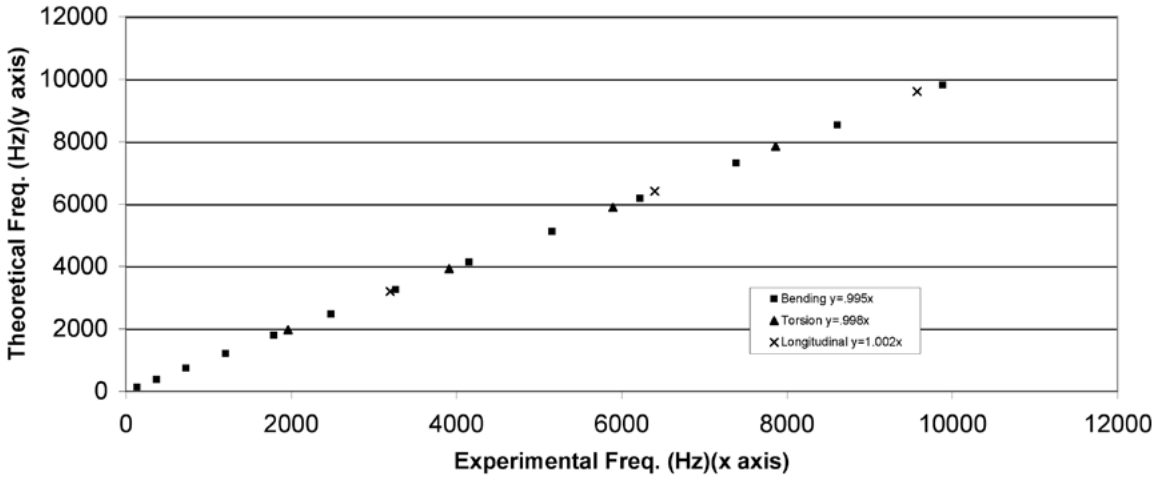

Fig. 12 Theoretical versus experimental natural frequencies of the free-free circular beam

Using the elastic modulus determined from the bending vibration, the linear curve fit of the theoretical and experimental longitudinal natural frequencies results in a line of slope 1.002 (Fig. 12). All these slopes are nearly one.

The first 20 measured natural frequencies of the free-free circular beam are given in Table 7, along with the natural frequencies from the Timoshenko and Euler-Bernoulli beam theories for the bending modes and vibration theories for the longitudinal and torsional modes. The Timoshenko beam theory gives a much better estimation of the higher bending natural frequencies than the Euler-Bernoulli beam theory. It is noted that, however, for the first two bending modes the Euler-Bernoulli beam theory gives a slightly better estimation.

The MAC matrices for the first 10 modes of the free-free circular beam, in the order of increasing frequencies, are calculated using the Euler-Bernoulli and Timoshenko beam theories, respectively, as shown in Tables 8 and 9, where the first seven modes are the bending modes, the eighth mode is the first longitudinal mode, and the ninth and tenth modes are the first two torsional modes. The MAC numbers for all the bending modes and the longitudinal mode are above 90%. The two beam theories yield essentially the same results for the MAC numbers, and the difference between the two is at most .01%. The normalized experimental mode shapes of the first ten modes of the free-free circular beam are plotted with the corresponding theoretical mode shapes in Figure 12.

Using a roving accelerometer test to find the mode shape of the longitudinal mode would result in a MAC number of .77 due to the mass loading effect. The movement of the accelerometer changed the natural frequency of the longitudinal modes by up to .8%. This change is not considered acceptable since a change of .8% corresponds to a frequency change of about 25 Hz for the first longitudinal natural frequency, which is about 20 times larger than the frequency resolution used. The roving hammer test yields much better results. The bracket (Fig. 11) used for the torsional modes gives good results for the natural frequencies but less accurate results for the mode shapes. The main reason for this is that repeatability is difficult to achieve, since it is hard to impact the beam at the same angle at each location in order to excite the torsional modes. An interesting observation from Tables 8 and 9 is that the first longitudinal mode and the first torsional mode are highly correlated, and so are the first

Bending Modes

Exp. (Hz)	Theo. (Hz) Euler	Dif. %	Theo. (Hz) Timoshenko	Dif. %
136.38	136.38	0	136.17	0.2
373.9	375.95	-0.5	374.34	-0.1
730	737	-1	730.9	-0.1
1206	1218	-1	1202	0.3
1792	1820	-1.6	1784	0.4
2482	2543	-2.5	2472	0.4
3268	3386	-3.6	3262	0.2
4157	4349	-4.6	4150	0.2
5156	5433	-5.4	5129	0.5
6225	6637	-6.6	6193	0.5
7384	7961	-7.8	7339	0.6
8609	9405	-9.2	8559	0.6
9887	10971	-11	9848	0.4

Torsional Modes			Longitudinal Modes		
Exp. (Hz)	Theo. (Hz)	Dif. %	Exp. (Hz)	Theo. (Hz)	Dif. %
1965	1961	0.20	3200	3201	-0.03
3915	3921	-0.15	6400	6402	-0.03
5896	5882	0.24	9578	9603	-0.26
7865	7842	0.29			

Table 7 Experimental and theoretical natural frequencies of the first 20 modes of the free-free circular beam

Exp. Mode	Theoretical Mode Number 1	2	3	4	5	6	7	8	9	10
1	96.2	0.1	16.3	0.0	13.5	0.9	8.1	2.3	1.2	85.6
2	0.7	99.0	0.0	11.2	0.3	9.2	0.3	25.9	16.2	1.3
3	19.9	0.0	99.3	0.1	8.7	0.1	1.7	0.0	0.3	13.5
4	1.0	13.3	0.0	99.6	0.1	4.1	0.5	4.4	18.3	2.8
5	8.4	0.2	7.1	0.1	96.3	1.2	1.1	1.9	8.1	28.1
6	0.3	4.0	0.2	4.0	0.7	93.6	0.1	4.6	0.9	0.7
7	9.0	0.0	2.2	0.0	2.5	1.8	98.0	3.5	0.4	6.3
8	0.7	24.7	0.0	9.7	1.0	1.3	0.5	90.6	83.8	0.3
9	0.7	24.7	0.0	9.7	1.0	1.3	0.5	90.6	83.8	0.3
10	95.2	0.1	27.6	0.0	10.1	0.7	6.0	2.1	1.4	85.0

Table 8 Free-free circular beam MAC matrix using the Euler-Bernoulli beam theory

Exp. Mode	Theoretical Mode Number 1	2	3	4	5	6	7	8	9	10
1	96.2	0.1	16.3	0.0	13.5	0.9	8.1	2.3	1.2	85.6
2	0.7	99.0	0.0	11.2	0.3	9.2	0.3	25.9	16.2	1.3
3	19.9	0.0	99.3	0.1	8.7	0.1	1.7	0.0	0.3	13.5
4	1.0	13.3	0.0	99.6	0.1	4.1	0.5	4.4	18.3	2.8
5	8.4	0.2	7.1	0.1	96.3	1.2	1.1	1.9	8.1	28.1
6	0.3	4.0	0.2	4.0	0.7	93.6	0.1	4.6	0.9	0.7
7	9.0	0.0	2.2	0.0	2.5	1.8	98.0	3.5	0.4	6.3
8	0.7	24.7	0.0	9.7	1.0	1.3	0.5	90.6	83.8	0.3
9	0.7	24.7	0.0	9.7	1.0	1.3	0.5	90.6	83.8	0.3
10	95.2	0.1	27.6	0.0	10.1	0.7	6.0	2.1	1.4	85.0

Table 9 Free-free circular beam MAC matrix using the Timoshenko beam theory

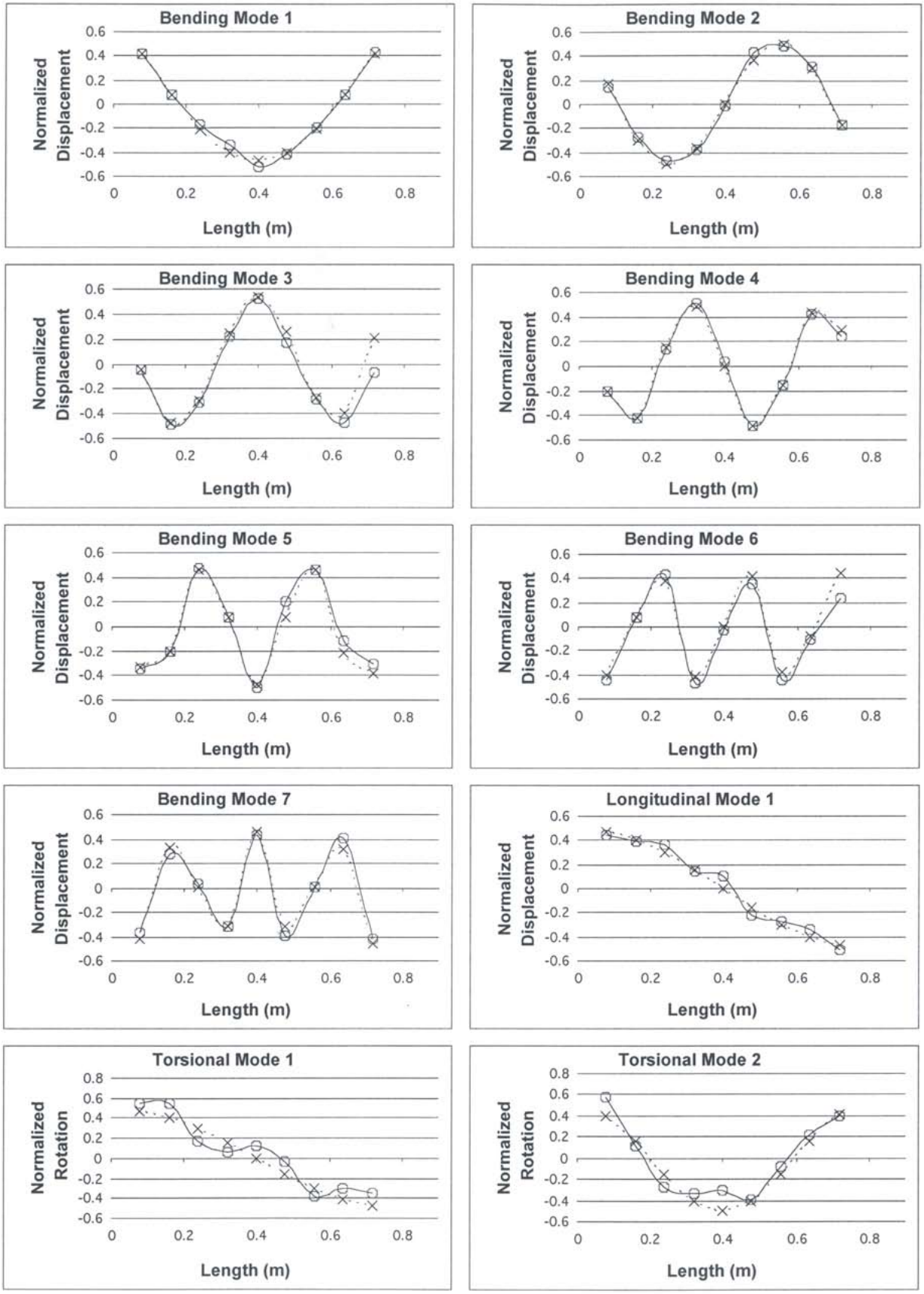

Fig. 13 The first ten theoretical (dashed line, -x-) and experimental (solid line, -o-) mode shapes of the free-free circular beam

bending mode and the second torsional mode. The reason for this is that in either case the two mode shapes are mathematically similar.

7. EDUCATIONAL VALUE

Much of the work presented in this paper can be used in the classroom or laboratory setting to aid both undergraduate and graduate students in learning the fundamentals of vibrations and experimental modal analysis. Students in most fields of engineering can benefit from learning that boundary conditions cannot be easily approximated in a physical system. The rectangular beam test stand can be used to demonstrate the effect of the bolt torque on the vibration of the beam. Students can also learn how to simulate the free-free boundary conditions from the circular beam test stand.

Different aspects of impact testing can be demonstrated with the two test stands. The choice of the hammer tip and extender can be demonstrated, as well as the selection of the excitation location. The concept of nodal points can be shown by placing the accelerometer on a node or impacting the beams at a node. The concept of mass loading can be demonstrated by examining how the natural frequencies change with the accelerometer location.

Methods for comparing the experimental and theoretical natural frequencies can be demonstrated along with the nondestructive ways to determine the material properties from these comparisons. Students can be shown why incorporation of rotary inertia and shear deformation is important for the higher modes of the circular beam. They also learn how to obtain the mode shapes from a series of experimental FRFs. The MAC number can be introduced to compare the mode shapes.

Students can see that due to existence of natural damping all the measured modes are complex, and can see the limits to which lightly damped and undamped natural frequencies and mode shapes can be compared. They can also learn about digital measurement and sampling techniques.

8. COURSE ACTIVITY AND STUDENT RESPONSE

The rectangular and circular beam test stands were demonstrated to students in the junior level Vibrations course (ENME360) at the University of Maryland, Baltimore County (UMBC) in the spring semester of 2004 and 2005. There were 44 students enrolled in the spring semester of 2004 and groups of 10 to 12 students were invited to attend the one-hour demonstration in the instructor's laboratory, the Dynamic Systems and Vibrations Laboratory (DSVL) at UMBC. The bending vibration of the circular beam was not discussed because the Timoshenko beam theory is not covered in the undergraduate vibrations course. The demonstration was also presented in a modified form to high school students in the Worthwhile to Help High School Youth (WORTHY) program administrated by Northrop Grumman in the summer of 2003 and those in the Future Engineers in Dynamic Systems (FEDS) Academy administrated by the DSVL in the summer of 2004 and 2005.

There are four main goals of the demonstration and accompanying student activity for ENME360. First is to have students become familiar with the equipment since most have never used this type before and need to understand the physics of the equipment. Second is to have students compare the differences between theoretical and experimental results and to understand the reasons for the differences or errors. Third is to have students find the material properties of the beams from the measured natural frequencies. Fourth is to have students understand how to design an experiment to measure the longitudinal and torsional vibration of the rectangular beam.

Students were guided through the basics of measuring the natural frequencies and mode shapes of the clamped-free rectangular beam. First, they were taught about the physics of an ICP shear accelerometer and different ways of mounting the accelerometer using Petro wax, dental cement, or stud mount. They were shown the calibration sheet for the accelerometer and explained the importance of taking precise measurement especially for mode shapes. Next, they learned how to use the ICP impact hammer with different tips and extender mass. They then learned the importance of a signal conditioner that converts the charge from the accelerometer and hammer to a voltage.

Students were introduced to the Siglab 20-42 spectrum analyzer, the types of measurements it can take, and the signals it can be used to generate. The relations among the measurement time, bandwidth, sampling frequency, and frequency resolution were explained. They were taught about the relevant windows for use with the impact test, such as force-exponential, box-exponential, and boxcar or no window. They learned that while the use of the exponential windowing can

avoid leakage, it can introduce extra damping into the measurement, which needs to be accounted for in post-processing for estimation of damping ratios. They were instructed to reject measurements that contained an overload since an overload is recorded as the maximum or minimum allowable voltage. Double hits were also rejected because a double hit can introduce dropouts in the input force spectrum that can lead to poor estimation of the FRF due to the noise inherent in the system [14, 15]. They need to be avoided especially when a force window is used because it can possibly exclude the second impact from the measurement. Students were taught how to setup the triggering for taking measurements with the Siglab, which if not done properly, makes it impossible or too easy to trigger a measurement. Students were also shown that some pre-triggering is important for satisfying the periodicity requirement of the Fast Fourier Transform (FFT) as it lets the measurement start at zero.

After the Siglab was set up, students were shown how a simple test is performed using three averages. The time history, FFT, FRF, and coherence were shown, and students were given a brief review of the FFT, FRF, and a short introduction to the coherence function. A second test was performed where one of the impacts was misplaced so that they could see the change in the time history, FFT, FRF, and coherence. A test was performed subsequently with the accelerometer at a different location, so students could see the effect of the accelerometer location on the dynamics of the system. The effect of the torque level on the clamp was also demonstrated, so students could see that the boundary conditions should not always be considered perfect even though the bolts seem to be tight.

Students were shown how to approximate the free-free boundary conditions with the circular beam. They were also shown how to measure and excite the second plane bending modes of the rectangular beam and the longitudinal and torsional modes of the circular beam. They performed a series of simple tests on their own to become more familiar with the equipment. They measured the mode shapes of the clamped-free beam using either the roving hammer technique or the roving accelerometer technique, followed by analysis and discussion on the advantages and disadvantages of each type of testing. Processing the FRF data in ME'Scope VES, students were shown that the structure has light natural damping with the measured phases close to 0 or 180 degrees. They were also shown how to animate the mode shapes of the beam, followed by a brief introduction to the MAC number and its importance in distinguishing one mode from another.

With the experimental data provided to students in the homework assignment, they determined the elastic modulus of the rectangular beam with clamped-clamped, clamped-pinned, and pined-pinned boundaries from the first 10 bending modes, and the elastic and shear moduli of the circular beam from the first three longitudinal and first four torsional modes, respectively. They were also asked to calculate the MAC matrices for the beams.

When the assignment was completed, students were surveyed to assess their opinions of the laboratory exercise. Five choices were provided for each of the four questions below: strongly agree, agree, neutral, disagree, and strongly disagree. Of the 33 students who responded in the spring semester of 2004 the majority agreed (67%) and strongly agreed (18%) that the demonstration helped bridge the gap between the theory and practice. The majority of the students also agreed (61%) and strongly agreed (9%) that the demonstration enhanced their understanding of the lecture material presented in class. When asked whether the demonstration stimulated thinking, 49% and 27% of the students agreed and strongly agreed, respectively. The introduction of the practical aspects of vibration measurement was found to be worthwhile and very worthwhile to 49% and 45% of the students, respectively.

9. CONCLUSIONS

The measured natural frequencies and mode shapes of the rectangular beam for each set of boundary conditions are in good agreement with the theoretical predictions. When the bending natural frequencies of the circular beam are used to determine its elastic modulus, the Timoshenko beam theory should be used. The Timoshenko and Euler-Bernoulli beam theories yield essentially the same mode shapes for the circular beam. The two test stands can be used to deliver a wide range of topics from the basics of vibrations to more advanced topics, such as Timoshenko beam theory, model/test correlation, and complex modal analysis. Survey results show that the test stands provide an effective teaching tool for introducing undergraduate students to vibration measurement and experimental modal analysis.

ACKNOWLEDGEMENTS

The authors wish to thank the support from the National Science Foundation through the award CMS-0116425 and the CAREER award CMS-0348605. The authors would like to thank Yan Chen for his assistance in the design of the rectangular beam test stand.

REFERENCES

1 Edward, N. S., The Role of Laboratory Work in Engineering Education: Student and Staff Perceptions. International Journal of Electrical Engineering Education, 2002, 39, pp. 11-19.

2 Grant, A. D. The Effective Use of Laboratories in Undergraduate Courses. International Journal of Mechanical Engineering Education, 1995, 23/2, pp. 95-101.

3 Wong, C. N., Zhu, W. D., and Xu, G. Y. On an Iterative General-Order Perturbation Method for Multiple Structural Damage Detection. Journal of Sound and Vibration, 2004, 273, pp. 363-386.

4 Zhu, W. D., Guo, B. Z., and Mote, C. D., Jr. Stabilization of a Translating Tensioned Beam Through a Pointwise Control Force. Journal of Dynamic Systems, Measurement, and Control, 2000, 122, pp. 322-331.

5 Hemanshu, P. R. and Alberts, T. E. Teaching Vibration Analysis using Symbolic Computation Software. The International Journal of Engineering Education, 1998, 26(2), pp. 75-88.

6 Kiritsis, N., Huang, Y. W., and Ayrapetyan, D. A Multi-Purpose Vibration Experiment Using Labview. Proceedings of the 2003 American Society for Engineering Education Annual Conference and Exposition, 2003, 1426, pp. 11472-11481.

7 Vlahinos, A. S. Importance of Experimental Structural Dynamics in Engineering Education. Proceedings 1985 Frontiers in Education Conference, 1985, 21A1, pp. 126-129.

8 Parker, R. Laboratory Exercises in Vibration for Mechanical Engineering Technology, 1995 American Society for Engineering Education Annual Conference Proceedings, 1995, 1647, pp. 798-806.

9 Cameron, T. and Russell, D. Laboratory Instruction in Acoustics and Vibration. 1996 American Society for Engineering Education Annual Conference Proceedings, 1996, 2526, pp. 2107-2111.

10 Zhu, W.D and Emory, B.H. On a Simple Impact Test Method for Accurate Measurement of Material Properties. Journal of Sound and Vibration, 2005, 287, 637-643.

11 Ewins, D. J. Modal Testing: Theory, Practice and Application, Second edition, 2000, (Research Studies Press LTD., Baldock, Hertfordshire, England), 171, pp. 415-437.

12 MatWeb.com - The Online Materials Database, Aluminum 6061-T6 and 6060-T651,<http://matweb.com/search/SpecificMaterial.asp?bassnum=ma6061t6>.

13 Standard test method for dynamic Young's modulus, shear modulus, and Poisson's ratio for advanced ceramics by impulse excitation of vibration. ASTM Designation C 1259-98, American Society for Testing and Materials, 1999.

14 Brown, D. Weaknesses of Impact Testing. Proceedings of the International Modal Analysis Conference - IMAC, 1997, 2, pp. 1672-1676.

15 Trethewey, M. W., and Cafeo, J.A. Tutorial: Signal Processing Aspects of Structural Impact Testing. The International Journal of Analytical and Experimental Modal Analysis, April, 1992, 7/2, pp. 129-149.

16 Inman, D. J. Engineering Vibration, Second edition, 2001, (Prentice Hall, Inc. Upper Saddle River, NJ), pp. 446-470.

17 Huang, T. C. The Effect of Rotatory Inertia and of Shear Deformation on the Frequency and Normal Mode Equations of Uniform Beams With Simple End Conditions. Journal of Applied Mechanics, December, 1961, pp. 579-584.

18 Stephen, N. G. Considerations on Second Order Beam Theories. Int. J. Solids Structures, 1981, 17, pp. 325-333.

Benjamin H. Emory is currently a Ph.D. student in the Department of Mechanical Engineering at the University of Maryland, Baltimore County, where he received his BS and MS degrees in Mechanical Engineering in 2003 and 2005, respectively. His research interest includes structural dynamics and structural health monitoring. He is a member of ASME, Society of Experimental Mechanics, and Tau Beta Pi honor society. His work has been supported by a National Science Foundation's Research Experiences for Undergraduates award, the Baltimore Gas and Electric Company, and a Graduate Assistance in Areas of National Need (GAANN) fellowship from the Department of Education. His interest in engineering education includes developing new test stands in dynamic systems for students at all levels.

Weidong Zhu is an Associate Professor in the Department of Mechanical Engineering at the University of Maryland, Baltimore County (UMBC), and the founder and director of its Dynamic Systems and Vibrations Laboratory. He received his double major BS degree in Mechanical Engineering and Computational Science from Shanghai Jiao Tong University in 1986, and his MS and Ph.D. degrees in Mechanical Engineering from Arizona State University and the University of California at Berkeley in 1988 and 1994, respectively. Prior to joining the UMBC in 1999, Dr. Zhu was an Assistant Professor at the Chinese University of Hong Kong and the University of North Dakota. He is a member of ASME and ASEE. His research spans the fields of dynamics, vibration, control, applied mechanics, and structural health monitoring, and involves analytical development, numerical simulation, and experimental validation. His interest in engineering education includes developing new STEM curricula for students at all levels. He is a recipient of the National Science Foundation's CAREER award.

The equation of motion for the bending vibration of a beam with constant cross-section and material properties is given by **[16]**

$$\frac{\partial^2 w(x,t)}{\partial t^2} + c^2 \frac{\partial^4 w(x,t)}{\partial x^4} = 0 \qquad \text{(A1)}$$

where w is the displacement at position x at time t, and c is given by

$$c = \sqrt{\frac{EI}{\rho A}} \qquad \text{(A2)}$$

in which I is the cross-sectional area moment of inertia, ρ is the mass per unit volume, and A is the cross-sectional area. Note that the variables in this paper, which are the same as those used earlier and not defined subsequently, have the same or similar meaning. The natural frequencies of the beam are

$$\omega_n = \beta_n^2 c \qquad \text{(A3)}$$

where the subscript n is the bending mode number and β_n is the solution to one of the following equations depending on the boundary conditions:

Free-Free and Clamped-Clamped

$$\cos(\beta_n l)\cosh(\beta_n l) = 1 \qquad \text{(A4)}$$

Clamped-Free

$$\cos(\beta_n l)\cosh(\beta_n l) = -1 \qquad \text{(A5)}$$

Clamped-Pinned

$$\tan(\beta_n l) = \tanh(\beta_n l) \qquad \text{(A6)}$$

Pinned-Pinned

$$\sin(\beta_n l) = 0 \qquad \text{(A7)}$$

in which l is the length of the beam. The mode shapes of the beam for different boundary conditions are:

Free-Free

$$Y_n(x) = D_n[\cosh(\beta_n x) + \cos(\beta_n x) - \sigma_n(\sinh(\beta_n x) + \sin(\beta_n x))] \quad \text{(A8)}$$

Clamped-Free, Clamped-Pinned, and Clamped-Clamped

$$Y_n(x) = D_n[\cosh(\beta_n x) - \cos(\beta_n x) - \sigma_n(\sinh(\beta_n x) - \sin(\beta_n x))] \quad \text{(A9)}$$

Pinned-Pinned

$$Y_n(x) = D_n \sin\frac{n\pi x}{l} \quad \text{(A10)}$$

where D_n are arbitrary constants, and σ_n are given by:

Free-Free, Clamped-Pinned, and Clamped-Clamped

$$\sigma_n = \frac{\cosh(\beta_n l) - \cos(\beta_n l)}{\sinh(\beta_n l) - \sin(\beta_n l)} \quad \text{(A11)}$$

Clamped-Free

$$\sigma_n = \frac{\sinh(\beta_n l) + \sin(\beta_n l)}{\cosh(\beta_n l) + \cos(\beta_n l)} \quad \text{(A12)}$$

The equations of motion from the Timoshenko beam theory are **[17]**

$$EI\frac{\partial^2\psi}{\partial x^2}+k\left(\frac{\partial y}{\partial x}-\psi\right)AG-I\rho\frac{\partial^2\psi}{\partial t^2}=0 \tag{B1}$$

$$\rho A\frac{\partial^2 y}{\partial t^2}-k\left(\frac{\partial^2 y}{\partial x^2}-\frac{\partial\psi}{\partial x}\right)AG=0 \tag{B2}$$

where y and ψ are the displacement and the slope of the deflection curve when the shear force is neglected, respectively, at position x at time t, and k is the shape factor for the cross-section. The boundary conditions for a free end are

$$\psi'=0 \tag{B3}$$

$$\frac{Y'}{l}-\psi=0 \tag{B4}$$

where the primes denote differentiation with respect to the non-dimensional length $\xi=\frac{x}{l}$ of the beam **[17]**. The solutions to Eqs. (B1) and (B2) are **[17]**

$$Y=C_1\cosh(b\alpha\xi)+C_2\sinh(b\alpha\xi)+C_3\cos(b\beta\xi)+C_4\sin(b\beta\xi) \tag{B5}$$

and

$$\Psi=C_1'\sinh(b\alpha\xi)+C_2'\cosh(b\alpha\xi)+C_3'\sin(b\beta\xi)+C_4'\cos(b\beta\xi) \tag{B6}$$

where C_1 through C_4 and C_1' through C_4' are constants. The frequency equation for the free-free beam is **[17]**

$$2-2\cosh(b\alpha)\cos(b\beta)+\frac{b}{(1-b^2r^2s^2)^{\frac{1}{2}}}\left[b^2r^2\left(r^2-s^2\right)+\left(3r^2-s^2\right)\right]\sinh(b\alpha)\sin(b\beta)=0 \tag{B7}$$

where

$$b^2=\frac{\rho Al^4\omega}{EI} \tag{B8}$$

$$r^2 = \frac{I}{Al^2} \tag{B9}$$

$$s^2 = \frac{EI}{kAGl^2} \tag{B10}$$

$$\frac{\alpha}{\beta} = \frac{1}{\sqrt{2}}\left\{ \pm\left(r^2 + s^2\right) + \left[\left(r^2 - s^2\right)^2 + \frac{4}{b^2}\right]^{\frac{1}{2}}\right\}^{\frac{1}{2}} \quad \text{for} \quad \left[\left(r^2 - s^2\right)^2 + \frac{4}{b^2}\right]^{\frac{1}{2}} > \left(r^2 + s^2\right) \tag{B11}$$

The numerical shape factor k for the circular cross-section is determined from **[18]**

$$k = \frac{6(1+\nu)^2}{7 + 12\nu + 4\nu^2} \tag{B12}$$

The mode shapes of the free-free beam can be calculated by applying the boundary condition in Eq. (B3) at $\xi = 0$ and $\xi = 1$ and that in Eq. (B4) at $\xi = 0$. Evaluating Eq. (B3) at $\xi = 0$ and using Eq. (B6) yields

$$b\alpha C_1' + b\beta C_3' = 0 \tag{B13}$$

Evaluating Eq. (B4) at $\xi = 0$ and using Eqs. (B5) and (B6) yields

$$\frac{b\alpha C_2 + b\beta C_4}{l} - C_2' - C_4' = 0 \tag{B14}$$

Evaluating Eq. (B3) at $\xi = 1$ and using Eq. (B6) yields

$$b\alpha C_1' \cosh(b\alpha) + b\alpha C_2' \sinh(b\alpha) + b\beta C_3' \cos(b\beta) - b\beta C_4' \sin(b\beta) = 0 \tag{B15}$$

The constants C_2' and C_4' are related to C_2 and C_4, respectively, through **[17]**

$$C_2' = \frac{b}{l}\frac{\alpha^2 + s^2}{\alpha} C_2 \tag{B16}$$

$$C_4' = \frac{b}{l}\frac{\beta^2 - s^2}{\beta} C_4 \tag{B17}$$

Substituting Eqs. (B16) and (B17) into Eq. (B14) yields

$$\frac{b\alpha}{l}C_2+\frac{b\beta}{l}C_4-\frac{b}{l}\frac{\alpha^2+s^2}{\alpha}C_2-\frac{b}{l}\frac{\beta^2-s^2}{\beta}C_4=0 \tag{B18}$$

Simplifying Eq. (B18) yields

$$\frac{C_2}{C_4}=\frac{\alpha}{\beta}\cong\lambda \tag{B19}$$

where a new variable λ is defined. The constants C_1' and C_3' are related to C_1 and C_3, respectively, through **[17]**

$$C_1'=\frac{b}{l}\frac{\alpha^2+s^2}{\alpha}C_1 \tag{B20}$$

$$C_3'=-\frac{b}{l}\frac{\beta^2-s^2}{\beta}C_3 \tag{B21}$$

By Eq. (B13) one has

$$\frac{C_1'}{C_3'}=\frac{-\beta}{\alpha} \tag{B22}$$

Substituting Eqs. (B20) and (B21) into Eq. (B22) yields

$$\frac{C_1}{C_3}=\frac{\beta^2-s^2}{\alpha^2+s^2}\cong\zeta \tag{B23}$$

where a new variable ζ is defined. Using Eqs. (B16), (B17), (B19)-(B21), and (B23) in Eq. (B15) yields

$$\begin{aligned}&\frac{b^2\left(\alpha^2+s^2\right)}{l}C_1\cosh(\alpha b)+\frac{b^2\left(\alpha^2+s^2\right)}{l}C_2\sinh(b\alpha)\\&-\frac{b^2\left(\beta^2-s^2\right)}{l\zeta}C_1\cos(\alpha b)-\frac{b^2\left(\beta^2-s^2\right)}{l\lambda}C_2\sin(b\beta)=0\end{aligned} \tag{B24}$$

Simplifying Eq. (B24) yields

$$\frac{-C_1}{C_2}=\frac{\left(\alpha^2+s^2\right)\sinh\left(\alpha b\right)-\left(\beta^2-s^2\right)\frac{1}{\lambda}\sin\left(b\beta\right)}{\left(\alpha^2+s^2\right)\cosh\left(\alpha b\right)-\left(\beta^2-s^2\right)\frac{1}{\zeta}\cos\left(b\beta\right)} \tag{B25}$$

Dividing the numerator and denominator of the right-hand side of Eq. (B25) by α^2+s^2 and using Eqs. (B19) and (B23) yields

$$\frac{-C_1}{C_2} = \frac{1}{\lambda\delta} \tag{B26}$$

where

$$\delta = \frac{\cosh(b\alpha) - \cos(b\beta)}{\lambda \sinh(b\alpha) - \zeta \sin(b\beta)} \tag{B27}$$

Setting $C_1 = 1$ and using (B19), (B23), and (B26) yields

$$C_2 = -\lambda\delta \tag{B28}$$

$$C_3 = \frac{1}{\zeta} \tag{B29}$$

$$C_4 = -\delta \tag{B30}$$

The mode shapes for the free-free beam can now be written as

$$Y_n(\xi) = D_n\left[\cosh(b\alpha\xi) - \lambda\delta \sinh(b\alpha\xi) + \frac{1}{\zeta}\cos(b\beta\xi) - \delta \sin(b\beta\xi)\right] \tag{B31}$$

It should be noted that this result is different from that given in **[17]**, which gives the coefficients for the hyperbolic sine and sine terms as being additive. Since λ, ζ, and δ are positive in this case, if the hyperbolic sine and sine terms in Eq. (B31) were additive as in **[17]**, an exponential curve would result for the mode shapes.

The equation of motion for the longitudinal vibration of a uniform beam is [**16**]

$$\left(\frac{E}{\rho}\right)\frac{\partial^2 u(x,t)}{\partial x^2} = \frac{\partial^2 w(x,t)}{\partial t^2} \tag{C1}$$

The free boundary conditions are

$$\begin{aligned}\frac{\partial u(0,t)}{\partial x} &= 0\\ \frac{\partial u(l,t)}{\partial x} &= 0\end{aligned} \tag{C2}$$

The longitudinal natural frequencies are

$$\omega_n = \frac{n\pi c}{l} \tag{C3}$$

where n is the mode number for the longitudinal vibration, and

$$c_l = \sqrt{\frac{E}{\rho}} \tag{C4}$$

is the longitudinal wave speed. The longitudinal mode shapes are

$$Y_n(x) = D_n \cos\frac{n\pi x}{l} \tag{C5}$$

The equation of motion for the torsional vibration of the circular beam is **[4]**

$$\frac{\partial^2 \theta(x,t)}{\partial t^2} = \left(\frac{G}{\rho}\right)\frac{\partial^2 \theta(x,t)}{\partial x^2} \tag{C6}$$

where θ is the rotation of the beam about the central axis at position x at time t, and G is the shear modulus. The free boundary conditions are

$$\begin{aligned}\frac{\partial \theta(0,t)}{\partial x} &= 0\\ \frac{\partial \theta(l,t)}{\partial x} &= 0\end{aligned} \tag{C7}$$

The torsional natural frequencies are

$$\omega_n = \frac{n\pi c}{l} \tag{C8}$$

where n is the mode number for the torsional vibration, and

$$c_t = \sqrt{\frac{G}{\rho}} \tag{C9}$$

is the torsional wave speed. The torsional mode shapes are

$$Y_n(x) = D_n \cos\frac{n\pi x}{l} \tag{C10}$$